Effect of remote field electromagnetic boundary conditions on microwave-induced plasma torches

M Jimenez-Diaz, J van Dijk, J J a M van Der Mullen

The effect of the remote field electromagnetic boundary conditions on microwave induced plasma torches

M Jimenez-Diaz[1], J van Dijk[1] and J J A M van der Mullen[1]

[1] Department of Applied Physics, Eindhoven University of Technology,
P.O. Box 513, 5600 MB, Eindhoven, The Netherlands.

E-mail: m.jimenez.diaz@tue.nl

Abstract. A flexible versatile electromagnetic model constructed with the PLASIMO platform is employed to explore electromagnetic features of microwave induced plasma torches. The bases, formed by a full-vector formulation of the Maxwell equations, provides the possibility to formulate the boundary conditions in a natural way. Together with the use of a direct matrix solver this gives a convergence speed-up of more than a factor of 100 when compared to a scalar formulation on the azimuthal magnetic field that uses an iterative solver. As a result this electromagnetic model is ready to act in future studies as part of the self-consistent description of plasma-electromagnetic coupling. With the electromagnetic model three types of configuration were studied: the closed, semi-open and open configurations, all three based on the same simplified model-plasmas. It is found that the closed configuration, acting as a cavity for which the (de)tuning is extremely sensitive for the plasma conditions, is less suitable for applications in which changes in plasma compositions can be expected. The semi-open configuration can be seen as a model for the practice often used in laboratories to place Microwave Induced Plasma torches in a grid that aims to protect the environment against microwave electromagnetic radiation. Calculations show that this is good practice provided the radius of this cylindrical grid is in the order of 90 mm. For the most often used configuration, the open version, we found that the power balance as expressed by the coefficients of absorption, transmission and reflection, depends on the electron density of the plasma. The reason is that the plasma acts as an antenna, that converts the electromagnetic waves from the co-axial structure to that of the expansion region and that this antenna function depends on the electron density. The influence of various other antenna elements is investigated as well.

Submitted to: *J. Phys. D: Appl. Phys.*

1. Introduction

Microwave Induced Plasmas [1] (MIPs) are interesting subjects for academic studies and offer many possibilities for industrial applications. The latter can be found in the fields of materials processing [2–4], gas volume cleaning [5] and for the construction of sources of ions [6], radicals [7] and photons [8].

Depending on the type of microwave coupling, MIPs can be divided into plasmas inside resonant cavities, surface-wave sustained plasmas and free expanding plasma torches. This paper is devoted to the last category for which we mention as examples the microwave plasma torch (MPT) [9] and the axial injection torch (TIA) [10]. In both cases the plasma is created in the zone where the transition takes place from the electromagnetic (EM) structure of a coaxial waveguide to that of an expansion zone. The expansion can take place in open air or in a vessel. The plasma gas, in most cases argon, is generally provided via the hollow inner conductor of the coaxial waveguide.

The working power of the TIA can reach 2 kW whereas a microwave plasma torch (MPT) is limited to around 200 W. This limitation is due to the use of coaxial cables instead of rectangular waveguides [9] as the connection to transfer the EM energy from the power supply to the torch.

In the past several experiments have been carried out on both MPT and TIA plasmas. Applying absolute intensity measurements [11,12] of atomic lines and the continuum it was possible to determine the electron density n_e and temperature T_e; these values have been compared with the results of the Stark intersection method and Thomson scattering [13–17]. Typical reported values for the TIA are $n_e = 3 \cdot 10^{21}$ m^{-3} and $T_e = 22000$ K. For the MPT the typical values are $n_e = 3 \cdot 10^{20}$m^{-3} and $T_e = 18000$ K (see [18]).

These properties of the electron gas were found to depend on experimental settings like the power level, the flow and the chemical composition of the gas flow (e.g. Ar versus He [19, 20]).

Especially the chemical composition was found to have an important impact and in line with this observation, it was understood that the internal plasma properties can also be changed by the entrainment of air. Oxygen and nitrogen molecules sucked in by the argon flow will enhance electron loss-mechanisms and will thus affect the properties of the electrons gas and the shape of the plasma flame. To study the effect of the environment, metallic plasma vessels were constructed in [11,18,21,22], with the purpose to change the gas-environment of the plasma (e.g. by replacing air by argon). It was found that chemical features of the environment indeed have an impact on the plasma. As explained in [13], when the plasma is created in a vessel filled with Ar, we get higher n_e- and lower T_e-values than when it is operated in air . Typical changes are an increase of n_e from $6 \cdot 10^{20}$ m^{-3} in air to $1.2 \cdot 10^{21}$ m^{-3} in argon and a change in T_e from 19000 K in air to 16000 K in argon. This was associated with an increase of the plasma radius from around 1.28 mm (air) to 1.79 mm (argon).

However the question rises in how far placing the plasma into a metallic gas-purification vessel will change the electromagnetic aspects of the plasma. A metal vessel placed around the plasma can cause back-reflection of the electromagnetic waves so that the electric field at the plasma location may change as well. More generally the question can be formulated *as in how far the electromagnetic features of the environment will change the properties of microwave induced plasma.* This question also addresses the impact of metallic grids that are sometimes placed around MIPs to avoid EM interferences with devices in the surroundings. It is not impossible that these grids will change the EM structure at the plasma location as well.

This study on the impact of the environment on the operation of MIP torches is based on numerical calculations. The modular toolkit PLASIMO [23, 24] was employed to calculate the fields for three different type of configurations; *open*, *semi-open* and *closed* systems; they are shortly denoted by, O, S or C configurations. The role of the plasma is played by a cylindrical bar or cone of given permittivity and conductivity.

Realizing that the plasma, formed at a tip of a nozzle has a radial size of less than 1 mm, while the vessels used in practice have radii of about 6 cm, the aim of this paper can be formulated as the question in *to what extend the remote‡ field EM boundary conditions will effect the operation*

‡ The distance of the EM boundaries to the plasma is far compared to the plasma radius but not large in comparison

and the inner part of a MIP.

In the past several numerical studies were published on one of the configurations O, S or C. In [25] a numerical EM study of the MPT is given. It deals with an *open* configuration. In [26] the coaxial microwave torch (CMT), i.e. a *semi-open* configuration (metal vessel working as a circular waveguide) was studied. After giving the EM module, it is also coupled with a plasma fluid model where flow, temperature and species equations in local thermal equilibrium are included. In [27] a *closed* configuration is used. It consists of a circular waveguide with a metal wall at the top (shortcut).

In all three studies cited above the EM field is found by solving a time-harmonic wave equation for the *azimuthal magnetic component* (i.e. an equation similar to the Helmholtz equation). In our approach we apply a full vector formulation instead, meaning that apart from the azimuthal magnetic component we also solve the radial and axial electric field components in a coupled manner. With this formulation and the use of the staggered Yee grid [28], the boundary conditions can be fulfilled in a more natural way, which, as we will see, speeds up the convergence process. Together with the application of a direct matrix-vector solver this leads to an enhancement of the convergence speed of more than a factor hundred as compared to the work of [27]. Another difference with the previous studies is that our study is not confined to just one configuration but that instead all three types of configurations, O, S and C are modelled and compared with each other. In this way a better understanding of the EM interplay of the plasma and the environment can be obtained. It was found that the O configuration is the most robust. This configuration is free from resonances so that a feed-back of the plasma on resonances can be avoided. Nevertheless we will see that the plasma still plays a role in the relative importance of the absorption, transmission and absorption of EM energy. The plasma has an antenna function in converting the wave from a TEM mode of the coaxial waveguide into that of radiation into open air. In order to get insight in this conversion the role of various antenna elements is investigated by changing the plasma density and the geometry of the transition region (gap).

This paper is organized as follows. Section 2 contains the definition of the configurations, the plasma and geometry of the setup. The physical and numerical model are explained in section 3. The results and discussion given in section 4. We end with the conclusions in section 5.

2. Configuration, Plasma and Geometry

The calculations were performed on a model structure that simplifies the basic EM structure of the TIA and MPT or more generally *MIP torches*. As stated above, both the TIA and MPT plasmas can be seen as extensions of the inner conductor of a coaxial waveguide, meaning that in both cases the plasma forms part of the EM transition from the coaxial waveguide to the expansion region. In the model we can take for this expansion zone a metallic free environment or a circular wave-guide. For the latter we can take various structures that can be divided into closed and semi-open circular waveguides. This leads to the following configurations:

C (Closed) The plasma expands into a closed circular waveguide, i.e. a circular wave guide with a shortcut at the end (see [18, 27]).

S (Semi-Open) The plasma expands into a open circular waveguide (see [26]).

O (Open) The plasma expands into open air (see [25]).

In selecting an appropriate model-plasma we are guided by the experimental values given in [29] and the observation given in [18, 25–27]. These are depicted in figure 1 where we see that, in practice, the plasma has two zones ([18]): an ionizing and a recombining zone. In constructing the model we confine ourselves to the active (ionizing) part where most of the electrons are found and we will assume that this model-plasma has the simple structure of a cylindrical bar, with a constant relative permittivity ϵ_r and conductivity σ (see section 3.1). The values of ϵ_r and σ are obtained from a simple model for the electron momentum balance [27, 30] that requires input

with the wavelength; We prefer use *remote* field rather than far-field to avoid confusion with the terms used in antenna theory where far-field is used for large distances compared to the wavelength.

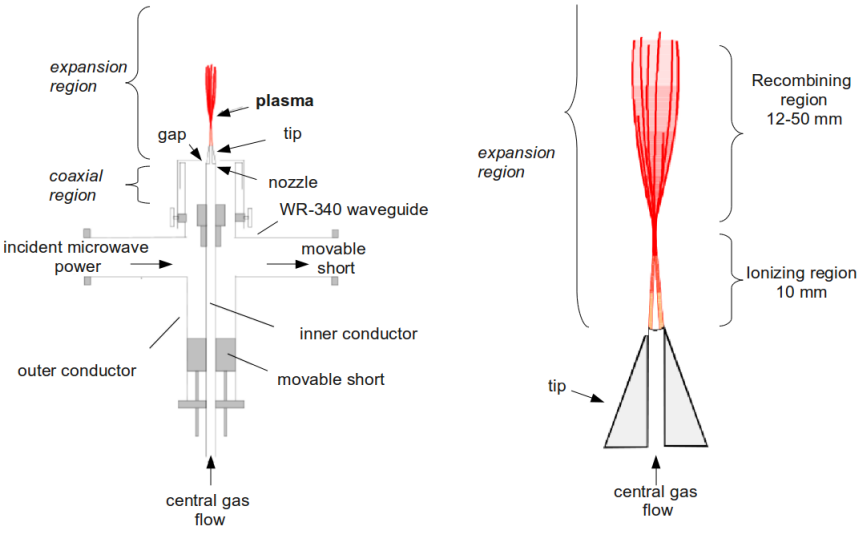

Figure 1. Left: a schematic view of a TIA. From the EM point of view the TIA basically consists of a coaxial structure placed perpendicular to a rectangular waveguide (WR-340). The plasma gas flows inside the inner conductor of the coaxial waveguide from the bottom via the nozzle to the expansion region. The EM energy generates the plasma just above the nozzle, thus in the region where the EM-transition takes place from the coaxial waveguide to the expansion region. Right: a schematic view of the two main plasma regions: the ionizing and recombining zone.

values for the electron density n_e, the elastic collision frequency ν_{eh} and the electromagnetic field frequency ω (see [31]). In the current study, we follow [32] in taking $\nu_{eh} = 100\omega$, with $\omega = 2\pi f$ while $f = 2.45$ GHz. The electron density is set to $n_e = 1 \cdot 10^{21}$ m^{-3}, except in section 4.2, where n_e is varied between 10^{20} m^{-3} and 10^{22} m^{-3} in a parameter study on the effect of n_e on the power response of the system.

2.1. Geometry

Figure 2(a) shows the geometry of the setup which exhibits a 2D axial-symmetric structure. Figure 2(b) depicts the structure of the corresponding computational grid. The coaxial waveguide has an inner radius $R_2 = 5.5$ mm, an outer radius $R_3 = 14.5$ mm and ends at $Z_1 = 100$ mm. The nozzle starts at Z_1, transforms into the tip at $Z_2 = 106$ mm and ends at $Z_3 = 118$ mm. The zone into which the plasma expands (in open air or into a circular waveguide) has a radius of R_4 and ends at Z_4, both of which are parameter in this study. These parameters values are given in table 1. As stated above, the plasma is located at the transition of the coaxial waveguide to the expansion region. As shown in figure 2(c), the plasma region is defined by the following (r,z)-values $(R_1, Z_3), (0, Z_3), (R_1, Z_p)$ and $(0, Z_p)$. Al the three configurations O, S, and C are described by the same geometry. The difference lies, as we will see, in the boundary conditions for the side and top of the circular waveguide.

3. Model

This section describes the electromagnetic model. The electromagnetic equations are given in section 3.1, the grid is given in section 3.2 while their respective boundary conditions are introduced in section 3.3. We will comment on the numerical implementation in section 3.4. A summary of

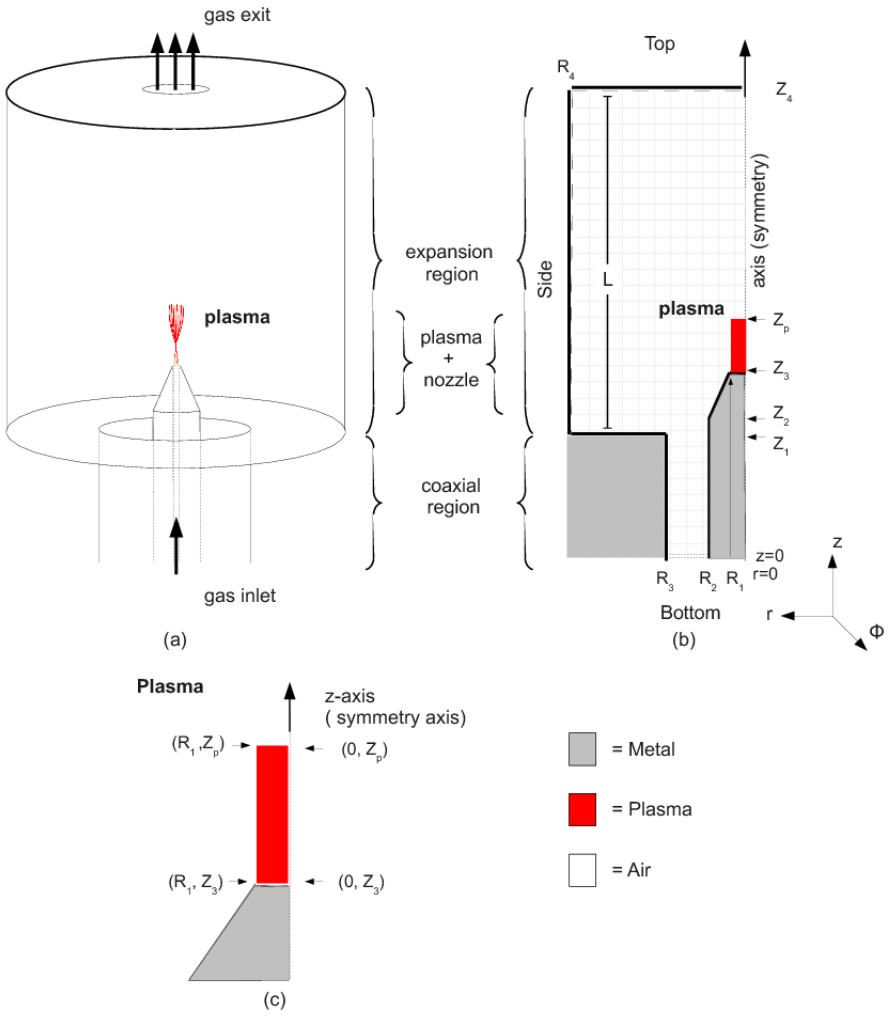

Figure 2. (a) the schematic geometry of the electromagnetic structure for the TIA showing 2D axial-symmetry; (b) the computational grid (see Table. 1 for values of geometry parameters); (c) detailed view of the model plasma, in this case a bar.

Parameters of the set-up			
Parameter	Value	Parameter	Value
R_1	1 mm	Z_1	100 mm
R_2	5.5 mm	Z_2	106 mm
R_3	14.5 mm	Z_3	118 mm
R_4	variable	Z_4	variable

Table 1. Parameter distances as used in the model-setup (see figure 2(b))

the model is given in Table 2 and a comparison with other models in Table 3.

Main characteristics of the current electromagnetic model	
Electromagnetic Problem	Deterministic (not the *modes* but the *fields* are determined) Harmonic fields ($\exp(i\omega t)$) 2D (symmetry axis along z, $\partial/\partial\phi = 0$) Full vector Maxwell Equations Transversal Magnetic (E_r, E_z, H_ϕ)
Projection	Finite Differences
Grid	staggered (Yee grid)
Ohm's law	$\vec{J} = \hat{\sigma}\vec{E}$
Solver	Direct Solver (superLU)

Table 2. Summary of the main characteristics of the electromagnetic model.

Main differences with other electromagnetic models				
	current	Bilgic [25]	Gritsinin [26]	Alves [27]
Fields (TM)	H_ϕ, E_r, E_z			
Equation (Comps.)	Full Vector (H_ϕ, E_r, E_z)	Azimuthal Magnetic Component (H_ϕ)		
Grid	Staggered (Yee)	Centered		
BC for	E_r, E_z	H_ϕ		
Torch	TIA, MPT and CMT	MPT	CMT	TIA
Different 'Gaps'	3	1	1	1
Configurations	C, S, O	O	S	C
Open Boundary at Exp. Reg.	Plane Wave Radial Wave	Plane Wave	Plane Wave	No
Solver	Direct	Direct	Iterative	Iterative
Grid Points, N	$\sim 10^5$	$\sim 10^4$	Not given	$\sim 10^4$
Comp. Time t_c	~ 6 s	Not given	Not given	~ 600 s

Table 3. Comparison of our electromagnetic model with those of [25], [26], and [27]. Here, TIA stands for *Torch à Injection Axiale* (Axial Injection Torch), MPT for Microwave Plasma Torch and CMT for Coaxial Microwave Torch.

3.1. Maxwell Equations

For a dissipative and non-magnetic linear medium and assuming harmonic time dependency $\exp(i\omega t)$, the Maxwell equations are

$$\nabla \times \vec{E} = -i\omega\mu_0\vec{H}, \tag{1}$$

$$\nabla \times \vec{H} = \vec{J} + i\omega\epsilon_r'\epsilon_0\vec{E}, \tag{2}$$

where $\vec{H}$, $\vec{E}$ and $\vec{J}$ are respectively the complex magnetic and electric fields and the current density, while ϵ_r' is the relative permittivity of the neutral and non-dispersive medium, ϵ_0 the vacuum permittivity and μ_0 the vacuum permeability. The angular frequency is $\omega = 2\pi f$ with f the EM wave frequency.

The axial symmetry is so that the electromagnetic quantities are azimuth-independent ($\partial/\partial\phi = 0$) and the problem can be described in two dimensions. This axial-symmetry is also refered to as the m = 0 mode.

The dimensions of the coaxial waveguide, R_2 and R_3, are selected so that only a transverse electromagnetic (TEM) mode can propagate. Due to the axial symmetry, $m = 0$, and because the expansion zone is being excited by a TEM mode where $H_z = 0$, only TM_0 modes are supported in the expansion zone [33–35]. This means that only the E_r, E_z and H_ϕ field components of a TM_0 mode are needed in the model.

We assume that the current density is determined by the electrons solely, and that it linearly depends on the electric field as expressed by Ohms' law, $\vec{J} = \hat{\sigma}\vec{E}$, where $\hat{\sigma}$ is the complex conductivity. The last, together with the harmonic assumptions, leads to the definition of the complex permittivity [31, 36]

$$\hat{\epsilon}_r = \epsilon_r' - i\hat{\sigma}(\epsilon_0\omega)^{-1}. \tag{3}$$

In the case of plasma $\epsilon_r' = 1$ and

$$\hat{\sigma} = \frac{\epsilon_0\omega_p^2}{\nu_{eh} + i\omega} \tag{4}$$

with the plasma frequency $\omega_p = \sqrt{e^2 n_e/m_e\epsilon_0}$ and ν_{eh} the collision frequency.

The complex conductivity [31, 36] in the plasma is obtained from the current density $\vec{J} = -en_e\vec{v}_e$ and the cold collisional electron approximation of the electron momentum balance equation for harmonic fields which reads

$$i\omega\vec{v}_e + \nu_{eh}\vec{v}_e = -\frac{e}{m_e}\vec{E}, \text{ thus } \vec{v}_e = \frac{-e\vec{E}}{m_e\left(\nu_{eh} + i\omega\right)}. \tag{5}$$

In this manner we show that $\vec{J} = \hat{\sigma}\vec{E}$ and obtain $\hat{\sigma}$.

With the above assumptions, the Maxwell equations included in the model get the form

$$\frac{\partial E_z}{\partial r} - \frac{\partial E_r}{\partial z} = k_0\tilde{H}_\phi, \tag{6}$$

$$\frac{\partial \tilde{H}_\phi}{\partial z} = k_0\hat{\epsilon}_r E_r, \tag{7}$$

$$\frac{1}{r}\frac{\partial r\tilde{H}_\phi}{\partial r} = -k_0\hat{\epsilon}_r E_z \tag{8}$$

where $k_0 = \omega\sqrt{\mu_0\epsilon_0}$ is the vacuum wavenumber, $\tilde{H}_\phi = iZ_0H_\phi$ the normalized azimuthal magnetic field component, and $Z_0 = \sqrt{\mu_0/\epsilon_0}$ the impedance of free space.

The time-averaged power density absorbed in the domain, Q (W/m^{-3}), is computed as

$$Q = \frac{1}{2}\mathrm{Re}\left(\vec{J}^*\vec{E}\right) = \frac{1}{2}\mathrm{Re}\left(\hat{\sigma}\right)|\vec{E}|^2. \tag{9}$$

So that the total power absorbed in volume V equals

$$P_{abs} = \int_V Q\mathrm{d}V = \frac{1}{2}\int_V \mathrm{Re}\left(\hat{\sigma}\right)|\vec{E}|^2\mathrm{d}V. \tag{10}$$

The complex Poynting vector is obtained in this case as

$$\vec{S} = \frac{1}{2}\vec{E}\times\vec{H}^* = \frac{1}{2}\begin{vmatrix} \hat{e}_z & \hat{e}_r & \hat{e}_\phi \\ E_z & E_r & 0 \\ 0 & 0 & H_\phi^* \end{vmatrix} = \frac{1}{2}E_r H_\phi^*\hat{e}_z - \frac{1}{2}E_z H_\phi^*\hat{e}_r, \tag{11}$$

and the time-average Poynting vector is

$$\bar{\vec{S}} = \mathrm{Re}(\vec{S}). \tag{12}$$

The conservation of electromagnetic energy is given by the Poynting theorem

$$\nabla\cdot\bar{\vec{S}} + Q = 0, \tag{13}$$

which in integral form reads

$$\oint_{\mathcal{B}} \left[\bar{\bar{S}} \cdot \vec{n}\right] db + P_{abs} = 0. \tag{14}$$

This merely states that the net§ power of the EM radiation entering the volume $\mathcal{V}$ enclosed by surface $\mathcal{B}$ (with outward normal vector $\vec{n}$) equals the power absorbed in $\mathcal{V}$.

3.2. Grid

Equations (6), (7) and (8), and the corresponding boundary conditions (see Section 3.3), are projected onto a staggered grid using finite differences following the method of Yee [28]. Figure 3(a). shows a cell for the Yee grid, where H_ϕ is defined at the nodal points and E_r and E_z at the edges of the grid cell. The location of the discrete fields components makes it possible to satisfy the continuity of the field at the edges. The computational grid is composed of *interior* and *boundary* cells. The electromagnetic fields are only solved in the interior cells. Each nodal point of an interior cell has, depending on the type of material, certain values of the permittivity ϵ_r and conductivity σ. In this study the materials used are *air* with $\epsilon_r' = 1$ and $\hat{\sigma} = 0$, and *plasma* for which $\epsilon_r' = 1$ and $\hat{\sigma}$ is given by equation (4). The values at possible interfaces between two interior cells are determined by interpolation. In the boundary cells, the electromagnetic field components are not solved. These cells are only used to set the *boundary conditions* for the adjacent *interior* cell. Boundary conditions are applied to the electric field components, E_r, E_z as they are the only field component defined at the interface of boundary cells and interior cell. They are described in section 3.3. The computational grid is stretched, meaning that the density of grid points is a function of radial position (see [37], [23]). The density of points close to the axis is six times higher than at radial edge of expansion zone.

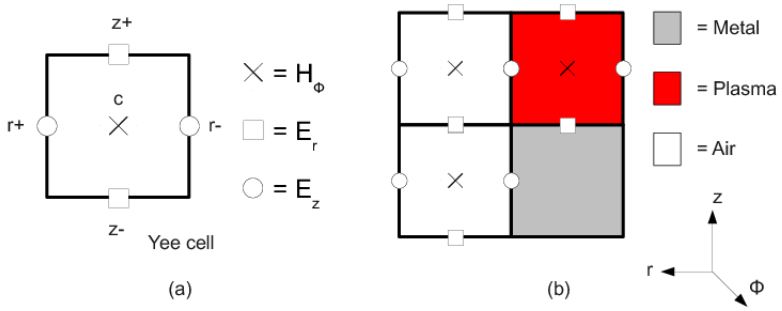

Figure 3. (a): general structure of a (Yee) cell used in the numerical method; (b): example of interfaces between different types of material cells.

.

3.3. Boundary Conditions

In general three different types of boundary conditions (BC) can be defined for a scalar field F at a surface $\mathcal{B}$

(i) Dirichlet: $F(\vec{x}) = p(\vec{x})$,
(ii) Neumann: $\vec{n} \cdot \nabla F(\vec{x}) = q(\vec{x})$,
(iii) Mixed: $\vec{n} \cdot [\nabla F(\vec{x}) + h(\vec{x}) F(\vec{x})] = w(\vec{x})$.

§ The *net* power entering a region refers to the power associated to the ingoing minus that of the outgoing waves.

Here $\vec{x}$ is the position vector of a point on $\mathcal{B}$, $\vec{n}$ the normal on $\mathcal{B}$ while $p(\vec{x})$, $q(\vec{x})$, $h(\vec{x})$, and $w(\vec{x})$ are explicitly known functions of $\vec{x}$. If $p(\vec{x})$, $q(\vec{x})$ or $w(\vec{x}) = 0$ for all $\vec{x} \in \mathcal{B}$, the BC is named *homogeneous*, otherwise the boundary is called *inhomogeneous*.

	Homogeneous	Inhomoneous
Dirichlet	Perfect Electric Conductor (PEC)	
Neumann	Axis	
Mixed	Propagation Boundary Condition (PBC)	Excitation

As stated above we only need to consider the BCs of the field components E_r and E_z. So they can play the role of F given above. Below we will sketch the various types of boundaries of the configuration under study and the corresponding conditions imposed to E_r and/or E_z.

- *Symmetry-BC (r = 0).* The axial symmetry requires at the axis a homogeneous Neumann BC i.e. type (ii) with $F = E_z$, applied at positions $\vec{x} \in \{Z_p \leq z \leq Z_4, r = 0\}$ and $q(\vec{x}) = 0$; i.e.

$$\left.\frac{\partial E_z}{\partial r}\right|_{\vec{x}} = 0. \tag{15}$$

- *Perfect Electrical Conductors (PEC)-BC.* For metallic boundaries we assume that the E field component parallel to the surface is zero which demands for a homogeneous Dirichlet boundary conditions i.e. type (i) with $q(\vec{x}) = 0$. For example at the inner conductor of the coaxial waveguide the condition reads

$$E_z|_{\vec{x}} = 0 \tag{16}$$

  at boundary positions $\vec{x} \in \{0 \leq z \leq Z_1, r = R_2\}$.

- *Propagation boundary condition (PBC) for axial propagation*‖. A homogeneous mixed boundary, i.e. type (iii), is used at the top-boundary positions $\vec{x} \in \{z = Z_4, 0 \leq r \leq R_4\}$, of the S and O configuration with $F = E_r$, $q(\vec{x}) = i\beta$, and $w(\vec{x}) = 0$. Thus

$$\frac{\partial E_r}{\partial z} + i\beta E_r = 0. \tag{17}$$

  Here β is the wavenumber of the wave. With this axial PBC, we assume that the EM energy leaves the domain in axial direction with a wave in the TM_{01} circular waveguide mode (see [39]) with wavenumber $\beta = \sqrt{k^2 - (p_{01}/R)^2}$, in which R is the radius of the circular waveguide, $k = \omega\sqrt{\mu_0\epsilon_0\epsilon_r}$ the wavenumber of the medium, while $p_{01} = 2.405$ is the first zero of the Bessel function J_0 of first kind [40]. Note that this boundary condition assumes a plane wave propagating in the positive z-direction $E_r \propto \exp(-i\beta z)$. This boundary condition is described in detail in [38, 41, 42].

- *PBC at side-boundary for the radial propagation.* A homogeneous mixed boundary (type (iii)) is used at the side-boundary $\vec{x} \in \{Z_1 \leq z \leq Z_4, r = R_4, \}$, for case O, with $F = E_z$, $q(\vec{x}) = k\dfrac{H_1^{\{2\}}(kr)}{H_0^{\{2\}}(kr)}$, and $w(\vec{x}) = 0$. Thus

$$\frac{\partial E_z}{\partial r} + k\frac{H_1^{\{2\}}(kr)}{H_0^{\{2\}}(kr)}E_z = 0 \tag{18}$$

  with H a Hankel function [40]. This BC, described in detail in [42], assumes an outward propagating radial wave with $E_z \propto H_1^{\{2\}}(kr)$.

- *Excitation-BC.* This inhomogeneous mixed BC, used at the bottom boundary $\vec{x} \in \{z = 0, R_2 \leq r \leq R_3\}$, has two components, one for the incident and one for the reflected wave. We

‖ This BC is often referred to as the absorbing BC (see [38]), however since we use absorption in another meaning and since this BC deals with the propagation of the wave outside the domain we prefer to call this the Propagation BC

assume that incident power driven into the plasma has a TEM mode so that the corresponding E-field component reads

$$E_r|^+(r,z) = \frac{C_{\mathrm{TEM}}}{r}\exp(-i\beta z) \tag{19}$$

with $C_{\mathrm{TEM}} = \sqrt{Z_0|P_i|/\pi/\ln(R_3/R_2)}$, and $|P_i|$, the (imposed) incident power. Due to the discontinuity present in the domain the incident wave will generate a wave that is reflected back to the entrance. For the corresponding component E_r^- we apply a PBC such that

$$\frac{\partial E_r^-}{\partial z} - ikE_r^- = 0. \tag{20}$$

In this case the wavenumber for the TEM mode coincides with the medium wavenumber, k. Note that this BC imposes at the entrance a plane wave propagating in the negative z-direction i.e. $E_r^- \propto \exp(+ikz)$. This is the opposite to the top boundary where $\exp(-i\beta z)$ is used instead. As the BC should be applied to the total E_r field, we substitute the relation $E_r^- = E_r - E_r^+$ into equation (20), which, using (19), gives

$$\frac{\partial E_r}{\partial z} - ikE_r = -2ik\frac{C_{TEM}}{r}\exp(-ikz). \tag{21}$$

As we can see the excitation- BC is of type (iii) with $F = E_r$, $q(\vec{x}) = ik$, and $w(\vec{x}) = 2ikC_{TEM}exp(-ikz)/r$.

To summarize, we give an overview of the BC of the three types of configurations C, S, and O (figures 4(a), 4(b) and 4(c), respectively) The configurations have in common the excitation-BC at the entrance of the coaxial waveguide, the PEC-BC at the inner and outer metallic walls of the coaxial waveguide and the symmetry-BC at the central axis of the expansion region. The differences are (see figure 4):

C. Closed the PEC-BC are applied at the side- and top- boundaries,

S. Semi-open the PEC-BC is applied at the radial side while an PBC acts at the top,

O. Open PBCs are applied to both the side (radial PBC) and top boundaries (axial PBC).

3.4. Numerics

The discretisation of equations (6), (7) and (8) into the Yee grid [28, 31] generates a system of linear equations

$$\vec{A}\cdot\vec{v} = \vec{b} \tag{22}$$

where $\vec{A}$ is a matrix that represents the operator for the Maxwell equation and the boundary conditions, $\vec{v}$ a vector formed by the discrete electromagnetic field components located at the grid positions, and $\vec{b}$ the source vector related to the excitation BC.

The creation and management of the corresponding system of linear equations is performed using the LinSys library (see [23]). A direct solver (SuperLU, see [43]) is used to compute the solution of equation (22), i.e. the electromagnetic fields at the grid positions. From the distribution of the electromagnetic fields, the power density Q is computed using a discrete version of equation (9) and the total power is computed integrating it over the volume. The Poynting vector is computed using equation (11) for each grid cell.

The Poynting vector is integrated over the surface area at the boundaries of bottom (excitation) entrance, top, and lateral sides. This gives the net power through these boundaries which is used in section 4 to define the reflected and transmission power coefficients.

The energy conservation equation (14) is applied to each grid cell.

For a grid with $N \sim 10^5$, the computation time is $t_c \sim 10s$, with a numerical precision of 10^{-12}, more specifically for $N = 75932$ the problem is solved within $t_c = 4.94$ s in a desktop computer using a processor of type AMD PHENOM II X4 955 at 3.2 GHZ and 530 MB out of 8 GB of memory of type DDR3 at 1333 MHz. The operating system is Ubuntu 10.04. This makes the EM model adequate for a future application in a self-consistent description of the fluid and electromagnetic aspects of MIPs.

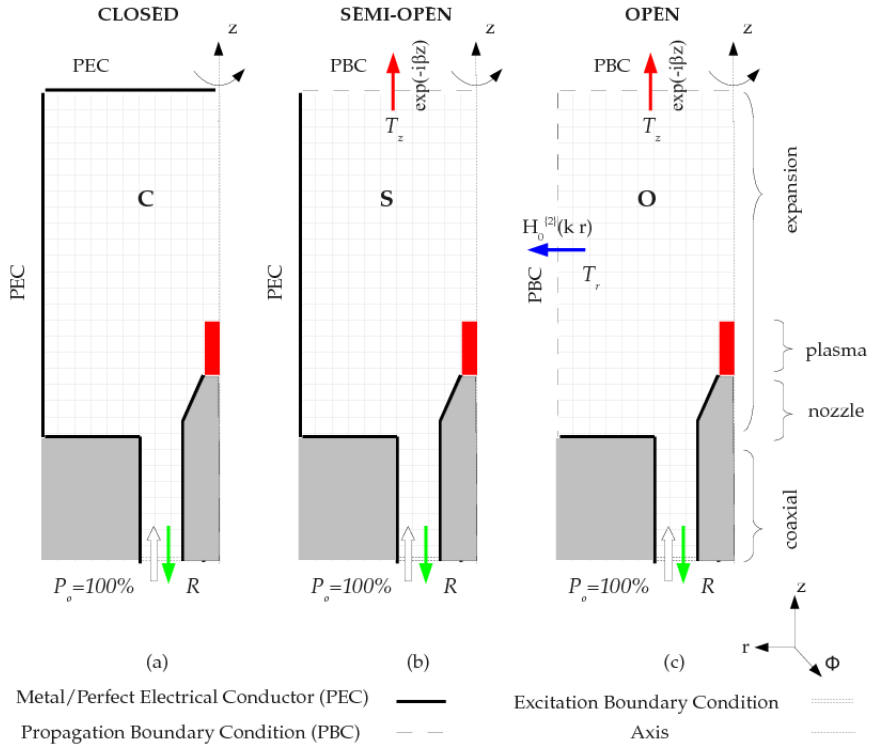

Figure 4. Different types of expansion regions: (a) Closed: a circular waveguide with short-cut at top i.e. a PEC-BC at the side and at the top, (b) Semi-Open: a circular waveguide open at the top side i.e a PEC-BC at the side and axial PBC at the top and (c) Open: Open air i.e. radial PBC at the side and axial PBC at the top.

4. Results and Discussion

In order to study the power response of the various torch configurations, we define at the excitation boundary the incident P_i and reflected power P_r. Together they form the *net power*, $P_{ns} = P_i + P_r$, supplied to the MIP. At the boundaries (of the domain) we have P_t, that is the power transmitted to the surroundings. This can be divided into $P_t = P_{t,z} + P_{t,r}$ thus the transmission at the top (axially emitted) and lateral side (radially emitted) (see figure 4). A *positive* sign refers to power *leaving* the domain (e.g. $P_{t,z}$ and $P_{t,r}$), whereas a *negative* sign refers to power *entering* the domain (e.g. P_i). Also P_{abs} is positive; the energy used for heating the electrons can be regarded as leaving the EM domain. With this sign-convention equation (14) transforms into

$$\sum P = P_i + P_r + P_t + P_{abs} = 0 \tag{23}$$

Substituting $P_i = -|P_i|$ and dividing all terms by $|P_i|$, equation (23) can be written as

$$1 = R + T + A \tag{24}$$

where $R = |P_r|/|P_i|$, $T = |P_t|/|P_i|$ and $A = |P_{abs}|/|P_i|$ are the reflection, transmission and absorption (power) coefficients of the configuration. The transmission coefficient can be further specified as $T = T_z + T_r$. The results given below are all based on simulations taking $|P_i| = 100$ W. The results of R, T, and A are obtained after normalizing the corresponding powers by $|P_i|$, thus dividing by 100 W. The relative importance of R,T and A will be denoted as the power response of the configuration.

4.1. Effect of the Remote Field Boundary Conditions

The power responses as functions of the vessel radius R_4 of the three different configurations C, S, and O are given in figures 5, 6 and 7. They have in common that the model-plasma has the same electron density $n_e = 10^{21}$ m^{-3} and shape: a cylindrical bar with a radius of 1 mm and an axial extension of 20 mm. The height of the expansion zone, $L = Z_4 - Z_1$, in all three cases equals 150 mm which corresponds to $Z_4 = 250$ mm. It should be noted, however, that only in the C-case the axial extend is limited by a physical (i.e. metallic) boundary. For the O- and S-cases the axial extend represents the position of the axial propagation BC. Mutatis mutandis the same applies to the radial extend as given by the R_4-value. In the C- and S- case this is a physical boundary, in the O- configuration the R_4-value represents the position of the radial propagation BC.

We can see in figure 5, that for the Closed configuration, the values for the transmission are absent. This is evident as the presence of both the radial and axial metallic limitation obstructs propagation. So only the values of the A- and R- coefficients remain. They strongly depend on the value of R_4. Strong absorption peaks ('resonances') are seen for $R_4 = 49$ mm, 78 mm and 98 mm. The positions of these peaks are comparable to those found with the analytical solution of a circular waveguides [27, 39]. However the presence of a plasma can change the positions and shapes of these peaks drastically. We can see this in figure 12, where curves A_1 and A_2 correspond to $n_e = 10^{21}$ and $5 \cdot 10^{21}$ m^{-3}, respectively, both with $\nu/\omega = 100$. Note how the increment in n_e modifies the position and strength of the absorption peaks.

Below a critical radius ($R_c = 47$ mm for $f = 2.45$ GHz) the character of the propagation changes and both C- and S- configurations share the same power response. The reason is that for $R < R_c$, the dispersion relation [32] provides an imaginary wavenumber and therefore only non-propagative solutions exist in the circular waveguide.

Another trend is found in the S-configuration as we can see in figure 6. There is no radial transmission across the metal wall, so that $T_r = 0$. Again the absorption and reflection depend on the radial position but this dependency is not so strong as in the C-case. The absorption peaks at $R_4 = 49$ mm and 78 mm found in the C case are no longer present; only a the broad absorption peak at $R_4 = 98$ mm is left over. Therefore, the operation of the torch around $R_4 = 98$ mm looks reasonable.

As we said before for $R < R_c$, both the S- and C-configurations behave the same due to the presence of non-propagating solutions.

For the O-configuration we see in figure 7, that the power emitted in axial direction can be neglected and that all the power response coefficients are more or less independent of the radius R_4 for $R_4 > 40$ mm. The latter can be seen as a validation of the propagation boundary condition as placed at R_4. However, for $R_4 < 40$ mm, the PBC is so close to the plasma that the electromagnetic wave is different from that assumed at the boundary and the reflections increases. Therefore the PBC formulated in equation (18) is not adequate for these low distances. Moreover, for $R_4 = 14.5$ mm the radial transmission becomes negative i.e. power *enters* from the side instead of *leaving*. Of course, this cannot happen in reality and so we have to conclude that it can not be used for so small values of R_4.

The relative change is defined as $\Delta f/f = \frac{\max(f)-\min(f)]}{\max(f)}$, with f = A,T, R. For $R_4 > 40$ mm, we find slight changes with a relative change $\Delta A/A = 3\%$, which is even lower for the range $R_4 > 80$ mm (where $\Delta A/A = 1\%$ is found) in T, A and R that can be attributed to the presence of numerical dispersion i.e. the wavenumber of the wave changes at it propagates through the numerical grid (see for instance section 3.4.4 in [44]). This can be improved with an optimum grid refinement (for a detail explanation on numerical dispersion for different spacial and time discretization schemes see [45]).

The low value of T_z for the O-configuration is better understood when looking to the radiation pattern of a monopole antenna close to a metal ground. As we can see in figure 8, the monopole antenna emits much more power in the radial than in the axial direction.

The figures 9, 10 and 11 show the influence of the axial extension of the expansion zone. In Figure 9, giving A and R as a function of $L = Z_4 - Z_1$ for the C-case, we see, just as in figure 5, sharp changes in A and thus R. The maximum in A takes place at $L = 150$ mm, which is the value

used for $Z_4 = 250$ mm in figures 5, 6 and 7.

For the O- and S-configuration, figures 7 and 6, we find only a slight dependence on Z_4, which again can be seen as a validation for propagation boundary condition performed at Z_4.

In the O- configuration, for $L > 124$ mm the relative change for the absorption is $\Delta A/A < 1\%$. Between 124 mm and 84 mm, $\Delta A/A \leq 3\%$. However, for $L = 64$ mm, the relative change becomes $\Delta A/A > 9\%$. This mean that the PBC is not adequate when placed at $L < 84$ mm i.e. a distance to the plasma of 54 mm for a plasma length of 20 mm.

In the S-Configuration, for L between 64 mm and 210 mm the relative change is less than 10%. This high relative change can be attributed to the presence of numerical dispersion ([44]).

The above makes clear that especially the closed configuration shows absorption peaks as functions of the sizes of the enclosure. In previous studies it was found that the dependency of the resonances on the dimensions of the enclosure, strongly depends on plasma conditions (see [27]). If for instance the cavity is tuned such that the power absorption is at maximum for a plasma driven in argon, it will be brought out of resonance if a small amount of H_2 or other molecular species is introduced. After such a change in plasma chemistry the cavity must be retuned. This implies that the C-configuration is not so suitable for plasma applications. It is illustrative to refer to the Evenson cavity [46] and the Beenakker cavity [47], which are not longer popular in spectrochemical analysis due to the resonances.

From now on we confine ourselves to the open case which indeed nowadays is the most often used configuration.

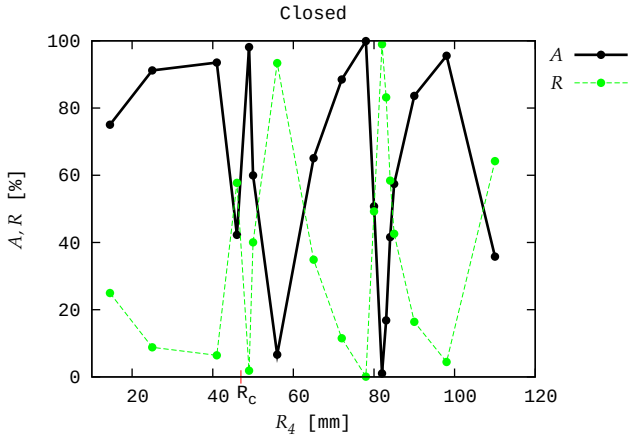

Figure 5. Power response of the Closed configuration with a bar-shaped plasma with of radius of 1 mm, axial extension 20 mm and an n_e-value of 10^{21} m^{-3}. The height of the expansion zone equals 150 mm which corresponds with $Z_4 = 250$mm; the absorption and reflection coefficients are given as functions of the radius R_4. As the configuration is closed the transmission is zero. Clear absorption peaks (resonances) can be seen at $R_4 = 49$ mm, 78 mm and 98 mm. For R_4 below the critical radius $R_c = 47$ mm, the behaviour is the same as in the Semi-open case because there is no propagating solution through the circular waveguide and the results are independent of the presence of a top metal wall.

4.2. Effect of the electron density value

As stated before the plasma is located at the transition region where the electromagnetic structure of the coaxial waveguide converts into that of the expansion region. In order to investigate in how far the plasma plays a role in this conversion we studied the power response of the open configuration as a function of the electron density. In all cases the plasma shape is fixed to that of a cylindrical bar with a radius and length of 1 mm and 20 mm respectively. The results, given in figure 13, show that, just as in figures 7 and 11, the transmission in axial direction can be neglected. Thus the dominant power channels are the radial transmission T_r, the absorption A

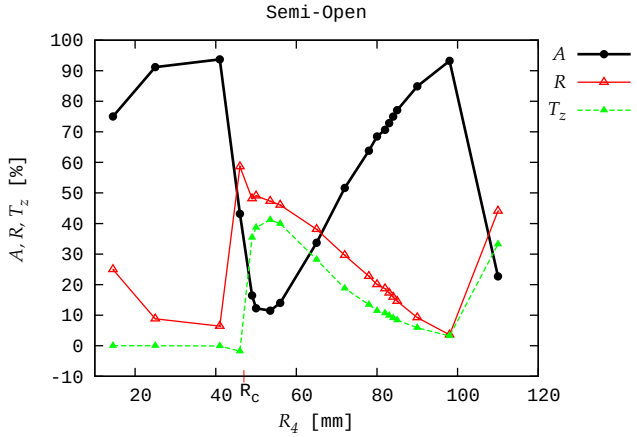

Figure 6. Power response of the Semi-open configuration with the same height and model plasma as that of figure 5; the absorption, reflection and transmission coefficients are given as functions of the radius R_4. As the configuration is closed in radial direction T_r is zero. Note that the absorption peaks at $R_4 = 49$ mm and 78 mm found in the C case are no longer present; only a more broad absorption peak at $R_4 = 98$ mm is left over. For R_4 below the critical radius $R_c = 47$ mm, the behaviour is the same as in the closed case because there is no propagating solution through the circular waveguide and the results are independent of the presence of a top metal wall.

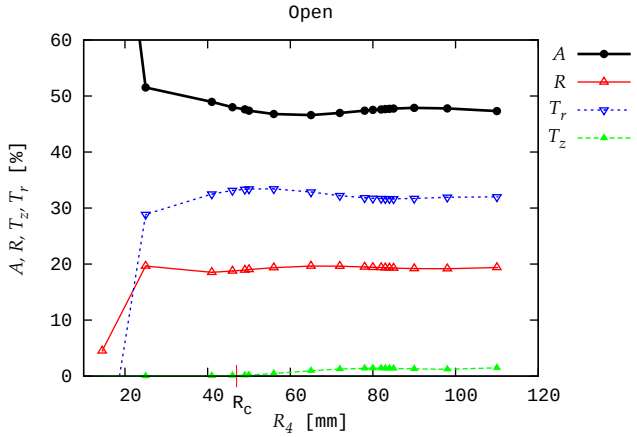

Figure 7. Power response of the Open configuration with the same height and model plasma as that used for figures 5 and 6; the absorption, reflection coefficients and transmission are given as functions of the radius R_4. Note that there are no absorption peaks for $R_4 \geq 40$ mm where the relative change is around 3%. For $R_4 < 40$ mm the propagation boundary condition is apparently not adequate. For $R_4 = 14.5$ mm the radial transmission even becomes negative i.e. power enters from the radial side. The Open-Configuration behaves as a monopole antenna near a ground metal (see figure 8) and this explains that T_r is much larger than T_z.

and reflection R. It is seen that, starting at $n_e = 10^{21}$ m^{-3} the A-value increases from 20 to almost 50% for increasing n_e and that this increase takes place at the expense of the R-value. Above $n_e = 10^{21}$ m^{-3} the radial transmission increases sharply thereby decreasing the A -value. Apparently the plasma serves as an antenna and the higher n_e, the better the antenna is.

However, the better the antenna function the less energy is left over for absorption. This sets an optimum value of the plasma density. At lower n_e-values more energy is absorbed thereby increasing the plasma density. However, due to this n_e-increase the plasma improves its antenna function, so that more energy is emitted and thus less is used for the absorption in the plasma.

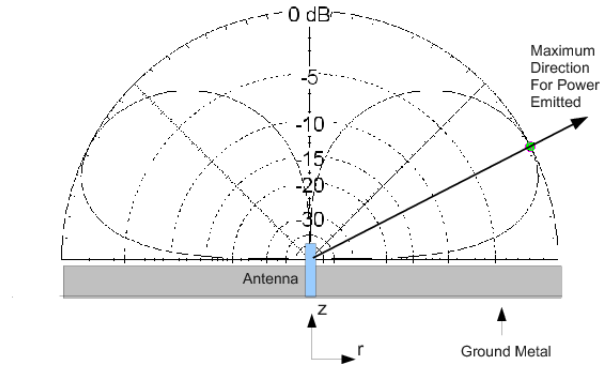

Figure 8. Radiation (transmission) pattern of a monopole antenna showing that an antenna close to a metallic ground transmits much more power in the radial than in the axial direction. Obtained using EZNEC (`http://www.eznec.com/`).

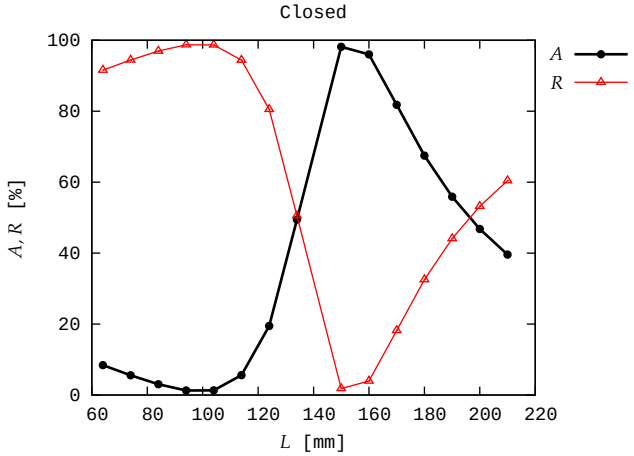

Figure 9. Power response of the Closed configuration with a bar-shaped plasma with of radius 1 mm, axial extension 20 mm and an n_e-value of 10^{21} m^{-3}. The radius of the expansion zone equals $R_4 = 55$ mm; the absorption and reflection coefficients are given as functions of the height of the expansion zone $L = Z_4 - Z_1$. As the configuration is closed the transmission is zero. Clear absorption peaks (resonances) can be seen at $L = 150$ mm.

This tends to decrease n_e which in turn leads to an increase in absorption. This negative feed-back might be (one of) the reason(s) for the fact that a MIP torch show an instable behavior.

4.3. Effect of the shape of the transition region (the 'gap')

In order to understand the antenna function we played with other elements of the *transition region*, hereafter shortly denoted as the *gap*. The possible structures are given in figure 14 where the model-plasma remains unaltered; it is bar-shaped with a electron density of 10^{21} m^{-3} while the radius and length are 1 mm and 20 mm, respectively. Figure 14(a) shows the influence of the extension of the inner conductor given by the insertion depth $d = Z_2 - Z_1$, figure 14(b) shows a perpendicular partial coverage of the gap, while figure 14(c) deals with an oblique partial coverage parallel to the tip of the inner conductor. The perpendicular coverage of figure 14(b) is inspired by [10] (see figure 1(a)). The oblique coverage is inspired by [48]. The results are schematically given in figure 15.

It is found that lowering the inner conductor from $d = 6$ mm to -6 mm leads to an enhancement of the reflection from about 20% to 31% but also that the absorption increases

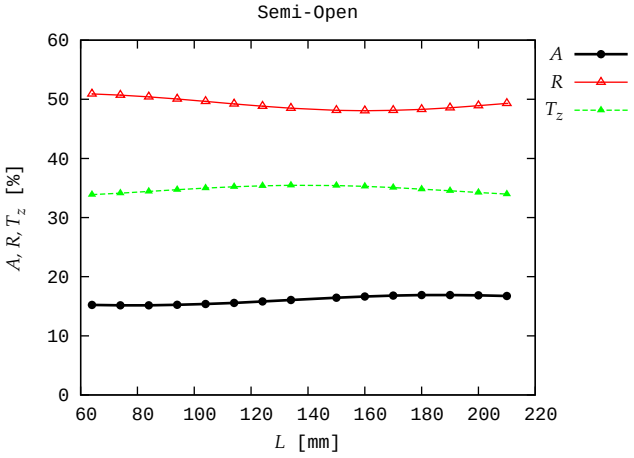

Figure 10. Power response of the Semi-open configuration with the same expansion zone radius and model plasma as that of figure 9; the absorption, reflection and transmission coefficients are given as functions of the height of the expansion zone $L = Z_4 - Z_1$. As the configuration is closed in radial direction T_r is zero. Note that the absorption peaks are not longer present and that the relative change is around 10%.

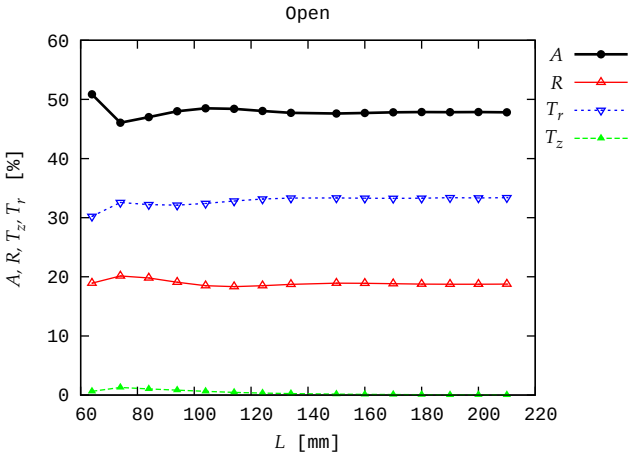

Figure 11. Power response of the Open configuration with the same expansion zone radius and model plasma as that of figures 9 and 10; the absorption, reflection and transmission coefficients are given as functions of the height of the expansion zone $L = Z_4 - Z_1$. The Open-Configuration behaves as a monopole antenna near a ground metal (see figure 8) and this explains that T_r is much larger than T_z. Note that the absorption peaks are not longer present and that for $L > 124$ mm the relative change for the absorption is $\Delta A/A < 1\%$. Between 124 mm and 84 mm, $\Delta A/A \leq 3\%$. However, for $L = 64$ mm or lower, the relative change becomes $\Delta A/A > 9\%$.

from about 46% to 55%. In figure 16, the extension of the nozzle is further reduced and even withdrawn into the outer cylinder of the coaxial waveguide. As we can see for $d < -25$ mm the complete plasma is hidden in the outer conductor wall and the power response is that of the C- and S-configurations, figures 5 and 6, for $R_4 = R_3 = 14.5$ mm. This operation seems lucrative since large absorption-values are obtained. However such a plasma in a cylinder is not very practical as it might cause ablation of the cylinder wall. Moreover, since the main plasma part will not operate in an open region, it will not be applicable for spectrochemical analysis or for the treatment of surfaces and volumes.

The coverage of the gap has a substantial effect on the reflection which changes from 20% (no coverage) to about 32% (oblique coverage) and 52% (horizontal coverage). So the negative effect

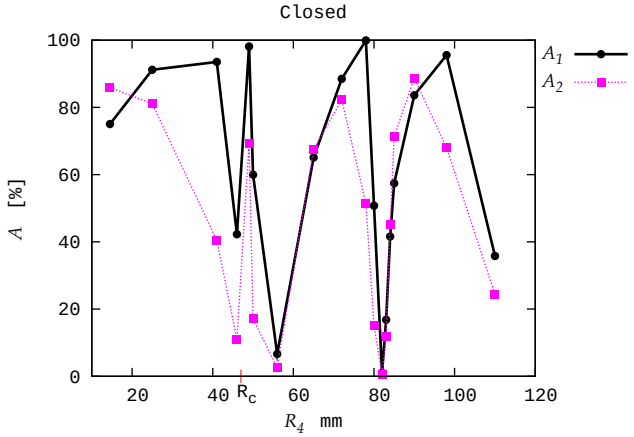

Figure 12. Absorbed power response as function of R_4 in the closed configuration with the same height as that of figure 5. The model plasma is the same with exception that n_e equals 10^{21} m^{-3} in A_1 and $5 \cdot 10^{21}$ m^{-3} in A_2. Note how the increment in n_e modifies the position and strength of the absorption peaks.

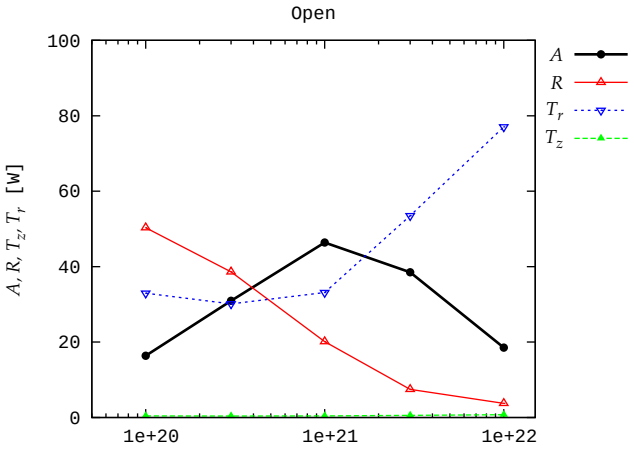

Figure 13. Power response of the Open configuration with the same expansion zone radius as that of figures 9 and same height of that of figures 5; the absorption, reflection and transmission coefficients are given as functions of the electron density n_e. At lower n_e-values more energy is absorbed thereby increasing the plasma density. However, due to this n_e-increase the plasma improves its antenna function, so that more energy is emitted and thus less is used for the absorption in the plasma. This tends to decrease n_e which in turn leads to an increase in absorption.

of coverage is that more power is send back to the magnetron power generator; the positive side is that from the net power admitted to the torch a larger fraction is absorbed by the plasma.

5. Conclusions

A flexible and versatile EM model is constructed using the PLASIMO platform [23, 24]. It is employed to explore the EM features of axi-symmetric microwave induced plasma (MIP) torches. The basis of the model is formed by the Maxwell equations used in a full vectorial form, meaning that for the TM mode the three vector components E_r, E_z and H_ϕ are solved in coupled manner. This is an important difference with most of the others methods found in literature for which the EM problem is described as a Helmholtz-like wave equation for the H_ϕ component solely.

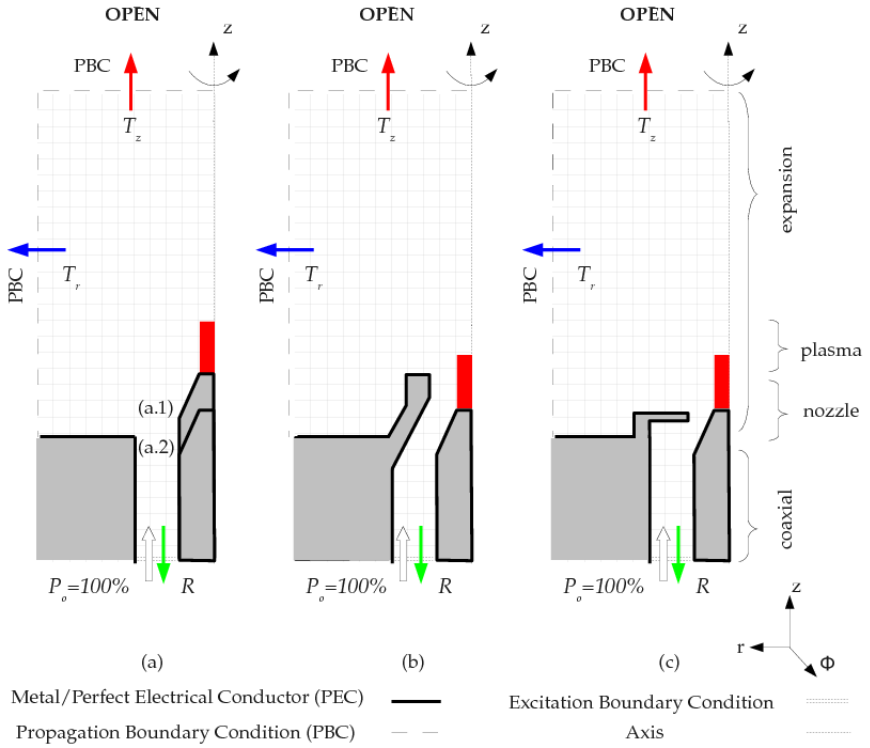

Figure 14. Different types of transition or 'gap-' regions: (a.1) Open gap with nozzle insertion of $d = Z_2 - Z_1 = 6$ mm, (a.2) Open gap with nozzle insertion of $d = -6$ mm, (b) Oblique Obstruction (similar to [48]) and (c) Obstruction perpendicular to the nozzle; similar to the gap in the TIA design [10] . The extension of the nozzle in (b) and (c) is that of (a.2). All of them are in O-configuration.

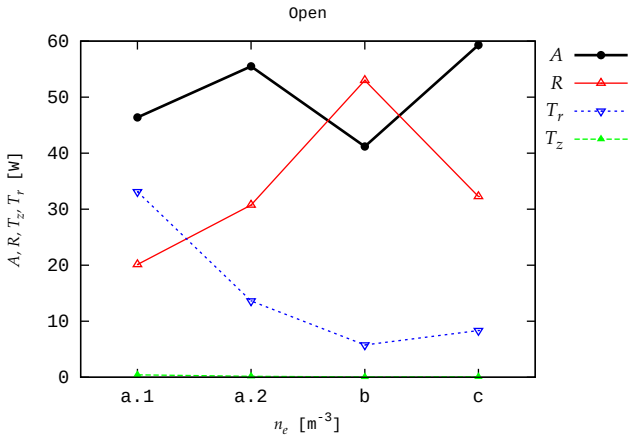

Figure 15. Power response versus the shape of the gap for the open configuration with the same expansion zone radius height of that of figures 13. (a.1) Open gap with nozzle insertion of $d = Z_2 - Z_1 = 6$ mm, (a.2) Open gap with nozzle insertion of $d = -6$ mm, (b) Oblique obstruction (similar to [48]) and (c) Obstruction perpendicular to the nozzle; similar to the gap in the TIA design [10] . The extension of the nozzle in (b) and (c) is that of (a.2). All of them are in O-configuration.

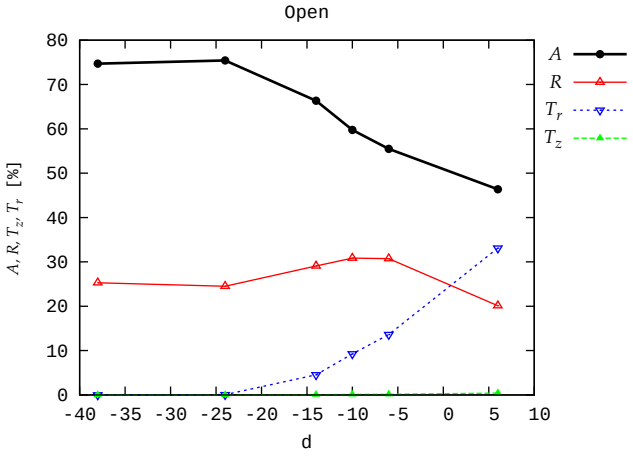

Figure 16. Power response versus the insertion depth $d = Z_2 - Z_1$ of the nozzle for the Open gap with the same expansion zone radius and height of that of figures 15. Lowering the inner conductor from $d = 6$ mm to -6 mm leads to an enhancement of the reflection from about 20% to 31% but also that the absorption increases from about 46% to 55%. For $d < -25$ mm the complete plasma is hidden in the outer conductor wall and the power response resembles that of the C- and S-configurations, figures 5 and 6, for $R_4 = R_3 = 14.5$ mm Note that $T_z = 0$, because the region below the outer conductor for z between Z_p and Z_3 acts as a circular waveguide which radius R_3 is below the critical radius $R_c = 47$ mm and therefore waves cannot propagate.

The full-vector approach has the advantage that the boundary conditions can be implemented in a natural way. This, together with the employment of a direct matrix solver, leads to a speed-up in convergence by a factor 100 when compared to [27]. For a grid of $N \sim 10^5$ cells the solution is reached in $t_c \sim 10$ s whereas the iterative process depicted in [27], demands $t_c \sim 10^3$ s for $N \sim 10^4$.

Three types of configurations were investigated; they are classified as Closed C-, Semi-open S- and Open -configurations. Changing from one configuration-type to an other is realized by simply changing the boundary condition of the expansion zone.

It is found that the C-configuration, for which the expansion takes place in a closed cylindrical cavity, strongly depends on the radial R and axial extension L. For various R- and L-values sharp resonances (strong absorption peaks) where found. Especially the radial sizes for which resonance are obtained are extremely sensitive to plasma features. This makes the C configuration less suitable for applications in the field for which (sudden) changes in the plasma conditions can be expected such as found in the field of spectrochemistry and the treatment of surfaces and volumes.

The features of the S-configurations, for which the wave expansion takes place in an open circular wave guide, are much less dependent of the sizes and therefore not so sensitive to plasma chemistry. These S-configuration can be seen as a model for the practice often used in laboratories to place MIP torches in a open cylindrical grid with the purpose to protect the environment against microwave EM radiation. Calculations show that this is good practice provided the radius of this grid is around 90 mm.

Most attention is paid to torches of the open configuration as these are most often used in practice. It is found that the power balance as expressed by the values of the absorption, transmission and reflection depends on the electron density of the plasma. The reason is that plasma is an essential element in the conversion of the EM waves of the co-axial structure to the EM-structure of the expansion region. This antenna function is better for increasing n_e- values. However, this implies that for increasing n_e the absorption decreases so that the plasma does not get enough energy to keep n_e high. This negative feed-back might be the reason for the instabilities often seen in the operation of open configured MIP torches.

Apart form the electron density we also investigated other aspects of the antenna- say gap-region. So for instance it is found that the plasma absorption strongly depends on the presence of a metallic obstruction placed at the end of the coaxial waveguide and the degree at which the

inner conductor of this coaxial waveguide extends into the expansion zone. The influence of two different gap obstructions were investigated namely a horizontal and an oblique one. It is found that these both enhance the reflection and absorption.

Due the flexibility of this EM model it can be used in future for further explorations of the impact of the various construction elements on the performance of torches and other types of MIPs. Moreover, it is ready to be used in combination with a set of transport equations to get a self-consistent description of the plasma-EM interaction.

Acknowledgments

This work is supported and funded by the Dutch Technology Foundation STW, the Eindhoven University of Technology and Draka Communications. The authors would like to thank A. Sola and A. Gamero from the University of Cordoba (Spain) for the fruitful discussions.

References

[1] Moisan M and Pelletier J 1992 *Microwave excited plasmas* volume 4 of *Plasma Technology* (Elsevier Science Publishers B.V.)
[2] Boulos M I, Fauchais P and Pfender E 1994 *Thermal plasmas: fundamentals and applications* (Plenum Press)
[3] Paquin L, Masson D, Wertheimer M R and Moisan M 1985 *Canadian Journal of Physics* **63** 831
[4] Küppers D and Lydtin H 1980 *Topics in Current Chemistry* **89** 107
[5] Airoldi V T, Borges C F M, Moisan M and Guay D 1997 *Applied Optics* **36** 4400
[6] Pomathiod L, Michau J L and Hamelin M 1988 *Review of Scientific Instruments* **59** 2409
[7] Montaser A and Golightly D 1992 *Inductively coupled plasmas in analytical atomic spectrometry* (VCH Publishers)
[8] Wharmby D O 1993 *Science Measurement and Technology IEE Proceedings A* **140** 465
[9] Jin Q, Zhu C, Borer M W and Hieftje G M 1991 *Spectrochimica Acta Part B Atomic Spectroscopy* **46** 417
[10] Moisan M, Sauve G, Zakrzewski Z and Hubert J 1994 *Plasma Sources Science and Technology* **3** 584
[11] Jonkers J, Vos H P C, van der Mullen J J A M and Timmermans E A H 1996 *Spectrochimica Acta Part B Atomic Spectroscopy* **51** 457
[12] Iordanova E 2010 *Poly-diagnostic validation of spectroscopic methods: in-depth monitoring of microwave induced plasmas* Ph.D. thesis Eindhoven University of Technology, The Netherlands
[13] Jonkers J, Selen L J M, van der Mullen J J A M, Timmermans E A H and Schram D C 1997 *Plasma Sources Science and Technology* **6** 533
[14] Prokisch C, Bilgiç A M, Voges E, Broekaert J A C, Jonkers J, van Sande M and van der Mullen J J A M 1999 *Spectrochimica Acta Part B Atomic Spectroscopy* **54** 1253
[15] van de Sande M J and van der Mullen J J A M 2002 *Journal of Physics D Applied Physics* **35** 1381–1391
[16] van der Mullen J J A M, van de Sande M, de Vries N, Broks B, Iordanova E, Gamero A, Torres J and Sola A 2007 *Spectrochimica Acta Part B Atomic Spectroscopy* **62** 1135–1146
[17] Álvarez R, Rodero A and Quintero M C 2002 *Spectrochimica Acta Part B Atomic Spectroscopy* **57** 1665
[18] Timmermans E A H 1999 *Atomic and molecular excitation processes in microwave induced plasmas a spectroscopic study* Ph.D. thesis Eindhoven University of Technology, The Netherlands
[19] van der Mullen J J A M and Jonkers J 1999 *Spectrochimica Acta Part B Atomic Spectroscopy* **54** 1017
[20] Álvarez R, Quintero M C and Rodero A 2005 *Journal of Physics D Applied Physics* **38** 3768
[21] Jonkers J, de Regt J M, van der Mullen J J A M, Vos H P C, de Groote F P J and Timmermans E A H 1996 *Spectrochimica Acta Part B Atomic Spectroscopy* **51** 1385–1392
[22] Timmermans E A H, Jonkers J, Thomas I A J, Rodero A, Quintero M C, Sola A, Gamero A and van der Mullen J J A M 1998 *Spectrochimica Acta Part B Atomic Spectroscopy* **53** 1553–1566
[23] van Dijk J, Peerenboom K, Jimenez M, Mihailova D and van der Mullen J J A M 2009 *Journal of Physics D Applied Physics* **42** 194012
[24] *http://plasimo.phys.tue.nl/*
[25] Bilgiç A M, Garloff K and Voges E 1999 *Plasma Sources Science and Technology* **8** 325–331
[26] Gritsinin S, Kossyi I, Kulumbaev E and Lelevkin V 2006 *Plasma Physics Reports* **32** 872–879
[27] Alves L L, Álvarez R, Marques L, Rubio S J, Rodero A and Quintero M C 2009 *The European Physical Journal Applied Physics* **46** 21001
[28] Yee K S 1966 *IEEE Transactions on Antennas and Propagation* **AP-14(8)** 302
[29] Jonkers J 1998 *Excitation and Transport in small scale Plasmas* Ph.D. thesis Eindhoven University of Technology, The Netherlands
[30] Hagelaar G J M, Hassouni K and Gicquel A 2004 *Journal of Applied Physics* **96** 1819–1828
[31] van den Donker M J 2008 *Modelling microwave plasmas for deposition purposes : exploring the freedom in space and chemistry* Ph.D. thesis Eindhoven University of Technology, The Netherlands
[32] Álvarez R and Alves L L 2007 *Journal of Applied Physics* **101** 103303

[33] Maloney J G, Smith G S and Jr. Scott W 1990 *IEEE Transactions on Antennas and Propagation* **38** 1059 –1068
[34] Noh Y C and Eom H J 1999 *IEEE Transactions on Microwave Theory and Techniques* **47** 2158–2161
[35] Harrington R F 2001 *Time-harmonic electromagnetic fields* IEEE Press Series on Electromagnetic Wave Theory (IEEE Press)
[36] Bowers K J 2001 *High frequency electron resonances and surface waves in unmagnetized bounded plasmas* Ph.D. thesis University of California, Berkeley
[37] Mobley C D and Stewart R J 1980 *Journal of Computational Physics* **34** 124
[38] Engquist B and Majda A 1977 *Applied Mathematical Sciences* **7, No. 5** 1765
[39] Pozar D M 1998 *Microwave engineering* (John Wiley & Sons, Inc) 2nd edition
[40] Abramowitz M and Stegun I A, eds 1965 *Mathematical handbook of functions* ((New York: Dover))
[41] Mur G 1981 *IEEE Transactions on Electromagnetic Compatibility* **EMC-23** 377–382
[42] Canning F X 1990 *IEEE Transactions On Antennas And Propagation* **38, No. 5**
[43] Demmel J W, Eisenstat S C, Gilbert J R, Li X S and Liu J W H 1999 *SIAM Journal on Matrix Analysis and Applications* **20** 720–755
[44] Rumpf R 2006 *Design and optimization of nano-optical elements by coupling fabrication to optical behaviour* Ph.D. thesis University of Central Florida Orlando Florida
[45] Liu Y 1996 *Journal of Computational Physics* **124** 396–416
[46] Fehsenfeld F C, Evenson K M and Broida H P 1965 *Review of Scientific Instruments* **36** 294–298
[47] Beenakker C I M 1976 *Spectrochimica Acta Part B Atomic Spectroscopy* **31** 483–486
[48] Kirichenko A, Motornenko A and Suvorova O 2003 *Plasma Physics Reports* **29** 528–533